Printed Circularly-Polarized Antenna with Ultra-Wide Axial-Ratio Bandwidth

Xiulong Bao
Technological University Dublin, xiulong.bao@tudublin.ie

Max Ammann
Technological University Dublin, max.ammann@tudublin.ie

Recommended Citation

Printed Circularly-Polarized Antenna with Ultra-Wide Axial-Ratio Bandwidth

Xiulong Bao and Max J. Ammann

Antenna & High Frequency Research Centre
School of Electronic & Communications Engineering,
Dublin Institute of Technology, Kevin Street, Dublin 8, Ireland

Ab*stract*— A circularly-polarized printed dipole-like antenna employing asymmetrical arms and an orthogonal slit in the ground plane is presented. It is fed by a stepped microstrip line which connects to the shorter arm. By utilizing surface currents on the asymmetrical arms and the orthogonal feedline structure, circular polarization is realised. Experimental and numerical data are in agreement and the measured results show a fractional impedance bandwidth of 41.3% (1.77 GHz to 2.69 GHz) and a wide axial-ratio bandwidth of 38.4 % (1.81 GHz to 2.67 GHz).

I. INTRODUCTION

The design of circularly-polarized antennas is becoming more attractive due to the increased number of applications in wireless communication and sensor systems, radio frequency identification (RFID), satellite communications and Global Navigation Satellite Systems (GNSS) [1-3]. Circular polarization (CP) is attractive compared to linear polarization because of reduced losses when arbitrary polarization misalignment occurs between the transmitter and receiver. CP can provide enhanced gain and cross-polar discrimination which improves the system's resilience to multipath fading effects.

Many microstrip patch antenna geometries providing CP have been reported in the literature [4-7] but with an axial ratio (AR) bandwidth typically less than 3%. In [8-11], investigations were carried out to develop dual-frequency CP antennas for satellite communications and GPS systems by using multiple-layer stacked patch structures. The development of modern GNSS and wireless systems currently demand antennas to provide CP performance over multiple narrow bandwidths, which introduces significant complexity, or alternately to provide a wideband CP performance. The GNSS systems typically requires AR bandwidths of 33% in order to cover from 1.15 GHz to 1.60 GHz and wireless and sensor systems require CP in the region of 1.7 GHz to 2.6 GHz. Recently, wideband CP performance with AR bandwidths in the region of 10% to 20% has been achieved using slot, loop, monopole and multilayer microstrip antennas [12-18].

Printed dipole antennas have been also reported due to their attractive features, which include broad bandwidth, low-profile and light weight. Series-fed dipole pairs have been used to provide bandwidths in excess of 30% for linearly polarized printed antennas [19] and recently, a printed dipole antenna with an integrated microstrip balun is reported with a very

wide impedance bandwidth of 45% for the linear-polarized element [20]. A novel CP crossed-dipole with a sequentially rotated configuration was reported to realize a 15% AR bandwidth [21]. A planar double L-shaped printed antenna with microstrip feed was shown to achieve dual-frequency operation [22]. The dual inverted-L antenna provided linear polarization for wireless applications. A printed dipole antenna providing a wide CP bandwidth of 23% using a microstrip-via balun was recently reported [23].

In this paper, a microstrip-fed printed asymmetrical dipole-like antenna which exploits a narrow slit in the ground plane to provide circular polarization is proposed. By adjusting the arm asymmetry and the length of the narrow slit in the ground plane between feedlines, a very wideband CP antenna is accomplished which yields a 3 dB AR bandwidth greater than 38%. In addition to the wide bandwidth, there is no via in this design, which reduces the cost and complexity. A parametric study was made in order to optimize the performance of the proposed antenna and the realization of a 38.4% AR bandwidth is detailed. The printed antenna was modeled, optimized, fabricated and tested, with its impedance and radiation characteristics measured. Good agreement is found between the simulated and measured results.

II. GEOMETRY OF THE PROPOSED PRINTED ANTENNA

The geometry of the antenna and the coordinate system are shown in Figure 1. The proposed antenna employs dipole-like asymmetrical arms and a ground plane with a narrow slit located in the centre. The ground plane is connected to the longer arm on one side of the substrate. A 50 Ω microstrip line connects to the shorter arm on the other side and is used to feed the antenna. The line width is stepped for improved broadband matching. The antenna is fabricated on a Taconic RF35 substrate with a relative permittivity of 3.5. The substrate loss tangent is 0.0018 and dimensions are 50 mm × 50 mm × 1.57 mm. The arrangement of surface currents on the dipole arms and on the orthogonal printed line provides right-hand circular polarization (RHCP) in the +z direction.

III. SIMULATION AND PARAMETRIC STUDY

The evolution of the antenna is described. Initially a simple antenna of the same dimensions without slit but with symmetrical arms of length 23.5 mm was modeled (Antenna A). The S_{11} is shown in Figure 2 to be narrowband. Antenna B employs asymmetrical arms (23.5 mm and 17.5 mm) and an upward shift is seen in the S_{11} with similar matching to the symmetrical case.

The introduction of the slit in ground plane (antenna C) to the symmetrical case improves both the matching and bandwidth. Employing asymmetry in the arm length is shown to give further improvement in bandwidth for the proposed antenna where a 41.3% impedance bandwidth is achieved. By comparison of the S11 curves, it is seen that the low frequency range is well matched by the introduction of the slit in the small ground. The high frequency range is extended by the additional asymmetry.

The impedance and AR bandwidth dependence on the antenna dimensional parameters

were studied numerically and the parameters which show the greatest effect on performance are discussed below. The key antenna parameters were found to be: the arm to ground plane separation Hs, the feedline width $W2$, the matching line length Ln, the short arm length $La2$, the length of the slit in the ground plane Ls and the ground plane dimensions Lg and Wg. The other antenna parameters were as follows: $La1 = 23.5$ mm, $Lw= 3.0$ mm, $W1=4.0$ mm, $W=3.0$ mm, $Lp=1.5$ mm.

A. The arm to ground plane separation Hs

The antenna tuning is dependent on this dimension and increasing the separation (with Lg & $W1$ constant) tunes the antenna resonant frequency downwards with small changes in AR bandwidth as shown in Figure 3(a) and (b). The value of $Hs =17.0$ mm provides both a wide impedance and AR bandwidth.

B. The feedline width $W2$

Figure 4(a) and (b) show the S_{11} and AR sensitivity to the width of the feed stripline. It is noted that this parameter has significant effects on both impedance and CP performance as $W2$ is changed from 5.5 mm to 9.5 mm. A width $W2 = 7.5$ mm is selected for best performance.

C. The matching line length Ln.

The 50 Ω microstrip line of width $W=3$ mm and length Ln connects to the SMA connector on one end and to the wider feedline of width $W2 =7.5$mm at the other end. A value of $Ln =15$mm is chosen for best matching while the AR is insensitive to this parameter as illustrated in Figure 5 (a) and (b).

D. The short arm length $La2$

The plots in Figure 6 show an increase in the upper edge frequency as the arm length $La2$ is decreased, with no change in the lower edge frequency ($W2$ remains constant at 7.5 mm). There is a corresponding decrease in AR bandwidth. The optimum value of arm length was chosen to be $La2=17.5$ mm.

E. The length of the slit in the ground plane Ls

Figure 7 displays the S_{11} curves for different values of the length of the slit in the ground plane Ls (with $Hs = 17.0$ mm). The slit length is a critical parameter for good performance. It can be seen that the impedance bandwidth increases as the slit length is increased, but the AR bandwidth is reduced. As a suitable compromise, the slit length is selected to be $Ls=6$ mm.

F. The ground plane size (Lg and Wg)

The proposed antenna performance is heavily dependent on the ground plane size. Figures 8 and Figure 9 display the dependence of the S_{11} and AR for different values of length Lg and width Wg. It is found that the AR is shows strong dependence on the ground plane width Wg as shown in Figure 9 (b). Due to the antenna sensitivity to groundplane and proximity effects, the antenna should be re-optimized for different groundplane sizes or when in close proximity to larger conducting structures.

IV. CIRCULAR POLARISATION MECHANISM

In order to explain the circular polarization mechanism of the proposed antenna, the simulated surface current distributions are presented. The direction of the surface currents on the antenna are illustrated in Figure 10 at a frequency of 2.2 GHz as the phase is changed from 0° through 270°. Figure 10(a) displays the surface current for the 0° phase reference and shows that the dominant radiating currents are along the –y direction, with the –x directed microstrip feedline currents opposing the x-directed currents on the ground connection for the longer arm. Figure 10(b) shows the surface current for the 90° phase and the dominant current flow is in the +x direction. The short and long arm currents oppose each other as well as the currents on the respective adjacent ground plane edges. Figure 10(c) represents the phase of 180° and shows a dominant +y directed current flow, with zero net radiating feedline current. Finally, for the 270° phase, the currents are directed in the -x direction, (phase inverted with respect to the 90° phase), hence, the polarization sense is RHCP in the +z direction. Furthermore, LHCP characteristics may be achieved by interchanging the long and short arm.

V. EXPERIMENTAL RESULTS

The proposed printed antenna shown in Figure 1 was fabricated with the following parameters selected: $La1$=23.5 mm, $La2$=17.5 mm, Ls=6.0 mm, Lw=3.0mm, Wg=50.0mm, Lg=18.0 mm, $W1$=4.0 mm, $W2$=7.5 mm, W=3.0 mm, Ln=15.0 mm, Lp=1.5 mm and Hs=17.0 mm. The S_{11} and AR were measured and are in good agreement with simulation as shown in Figure 11 and Figure 12. The results show a 10 dB return loss bandwidth of 920 MHz (1.77 GHz to 2.69 GHz) which represents a fractional bandwidth of 41.3% at the centre frequency of 2.233 GHz and a 3 dB AR bandwidth of 860 MHz or 38.4 % (1.81 GHz to 2.67 GHz).

The radiation patterns were measured and compare well to simulated data and are illustrated in Figures 13 to 15. The normalized patterns are shown for the *XZ* and *YZ* planes for three frequencies spread across the CP bandwidth, namely 1.85 GHz, 2.2 GHz and 2.55 GHz. The patterns show a broadside RHCP pattern with wide beamwidth. The measured peak gains are 2.2dBic and are stable across the band. The cross-polar rejection is typically better than 12dB.

VI. CONCLUSION

A single-layer printed antenna employing asymmetrical arms and a ground plane slit is shown to realize wideband circular polarization. By adjustment of the key dimensional parameters, the orthogonal modes on the antenna have the appropriate magnitude and phase relationship to provide circular-polarization with an axial-ratio bandwidth in excess of 38%.

REFERENCES

[1]. H.W. Kwa, X.M. Qing, and Z.N. Chen, Broadband Single-Fed Single-Patch Circularly Polarized Antenna for UHF RFID Applications, *IEEE Antennas and Propagation International Symposium*, July 2008, pp. 5-11.

[2]. O. Leisten, J.C. Vardaxoglou, P. McEvoy, R. Seager, and A. Wingfield, Miniaturised Dielectrically-Loaded Quadrifilar Antenna for Global Positioning System (GPS), *Electronics Letters*, Vol. 37, No.22, 2001, pp.1321-1322.

[3]. X.L. Bao, G. Ruvio, M.J. Ammann, M. John, A Novel GPS Patch Antenna on a Fractal Hi-Impedance Surface Substrate, *IEEE Antennas and Wireless Propagation Letters*, Vol. 5, 2006, pp. 323-326.

[4]. J.R. James and P.S. Hall, Handbook of Microstrip Antenna, London, U.K: Peter Peregrinus, 1989, Vol. 1

[5]. M.B. Oliver, Y.M.M. Antar, R.K. Mongia, and A. Ittipiboon, Circularly Polarized Rectangular Dielectric Resonator Antenna, *Electronics Letter*, Vol.31, No.6, 1995, pp.418-41

[6]. X.L. Bao, M.J. Ammann, Comparison of Several Novel Annular-Ring Microstrip Patch Antennas for Circular Polarization, *Journal of Electromagnetic Waves and Application*, Vol. 20, No.11, 2006, pp. 1427-1438.

[7]. K.F.Tong, and J.J.Huang, New Proximity Coupled Feeding Method for Reconfigurable Circularly Polarized Microstrip Ring Antennas, *IEEE Transactions on Antennas and Propagation*, Vol. 56, No. 7, 2008, pp.1860-1866

[8]. F. Ferrero, C. Luxey, G. Jacquemod, and R. Staraj, Dual-Band Circularly Polarized Microstrip Antenna for Satellite Applications, *IEEE Antennas and Wireless Propagation Letters*, Vol. 4, 2005, pp.13-15

[9]. Y.J.Zhou, C.C.Chen, and J.L.Volakis, Dual Band Proximity-Fed Stacked Patch Antenna for Tri-Band GPS Applications, *IEEE Transactions on Antennas and Propagation*, Vol.55, No.1, 2007, pp.220-223

[10]. L.I. Basilio, R. Chen, J.T. Williams, and D.R. Jackson, A New Planar Dual-Band GPS Antenna Designed for Reduced Susceptibility to Low-Angle Multipath, *IEEE Transactions on Antennas and Propagation*, Vol. 55, No. 8, 2007, pp.2358-2366

[11]. L.Boccia, G.Amendola, and G.Di Massa, A Dual Frequency Microstrip Patch Antenna for High-Precision GPS Applications, *IEEE Antennas and Wireless Propagation Letters*, Vol.3, 2004, pp.157-160

[12]. R.L. Li, V.F. Fusco, and H. Nakano, Circularly Polarized Open-Loop Antenna, *IEEE Transactions on Antennas and Propagation*, Vol.51, No.9, 2003, pp.2475-2477

[13]. Y.B.Zhang, and L.Zhu, Printed Dual Spiral-Loop Wire Antenna for Broadband Circular Polarization, *IEEE Transactions on Antennas and Propagation*, Vol.54, No.1, 2006, pp.284-288

[14]. C.J. Wang, Y.C. Lin, New CPW-fed Monopole Antennas with Both Linear and Circular Polarisations, *IET Microwaves, and Antennas and Propagation*, Vol. 2, No.5, 2008, pp.466-472

[15]. J.S. Row, The Design of a Squarer-Ring Slot Antenna for Circular Polarization, *IEEE Transactions on Antennas and Propagation*, Vol. 53, No. 6, 2005, pp.1967-1972

[16]. S. Shi, K. Hirasawa, and Z.N. Chen, Circularly Polarized Rectangularly Bent Slot Antennas Backed by a Rectangular Cavity, *IEEE Transactions on Antennas and Propagation*, Vol.49, No. 11, 2001, pp.1517-1524

[17]. S. Gao, Y. Qin, A. Sambell, Low-Cost Broadband Circularly Polarized Printed Antennas and Array, *IEEE Antennas and Propagation Magazine*, Vol. 49, No.4, 2007, pp.57-64

[18]. H. L. Chung, X. Qing, and Z. N. Chen, A broadband circularly polarized stacked probe-fed patch antenna for UHF RFID applications, *International Journal of Antennas and Propagation,* vol. 2007, Article ID 76793, 8 pages, 2007. doi:10.1155/2007/76793

[19]. F. Tefiku, and C.A. Grimes, Design of Broad-Band and Dual-Band Antennas Comprised of Series-Fed Printed-Strip Dipole Pairs, *IEEE Transactions on Antennas and Propagation*, Vol.48, No.6, 2000, pp.895-900

[20]. Q.Q. He, B.Z. Wang, and J. He, Wideband and Dual-Band Design of a Printed Dipole Antenna, *IEEE Antennas and Wireless Propagation Letters*, Vol.7, 2008, pp.1-4

[21]. J.W. Baik, K.J. Lee, W.S. Yoon, T.H. Lee and Y.S. Kim, Circularly Polarised Printed Crossed Dipole Antennas with Broadband Axial Ratio, *Electronics Letters*, Vol.44, No.13, 2008, pp.785-786

[22]. M.H.Yeh, Planar Double L-Shaped Antenna of Dual Frequency, US Patent, No. 6 801 168 B1.

[23]. X. L. Bao. P. McEvoy & M. J. Ammann, Microstrip-fed Wideband Circularly Polarized Printed Antenna, *IEEE Transactions Antennas & Propag.* 2010, 58, (10), (accepted).
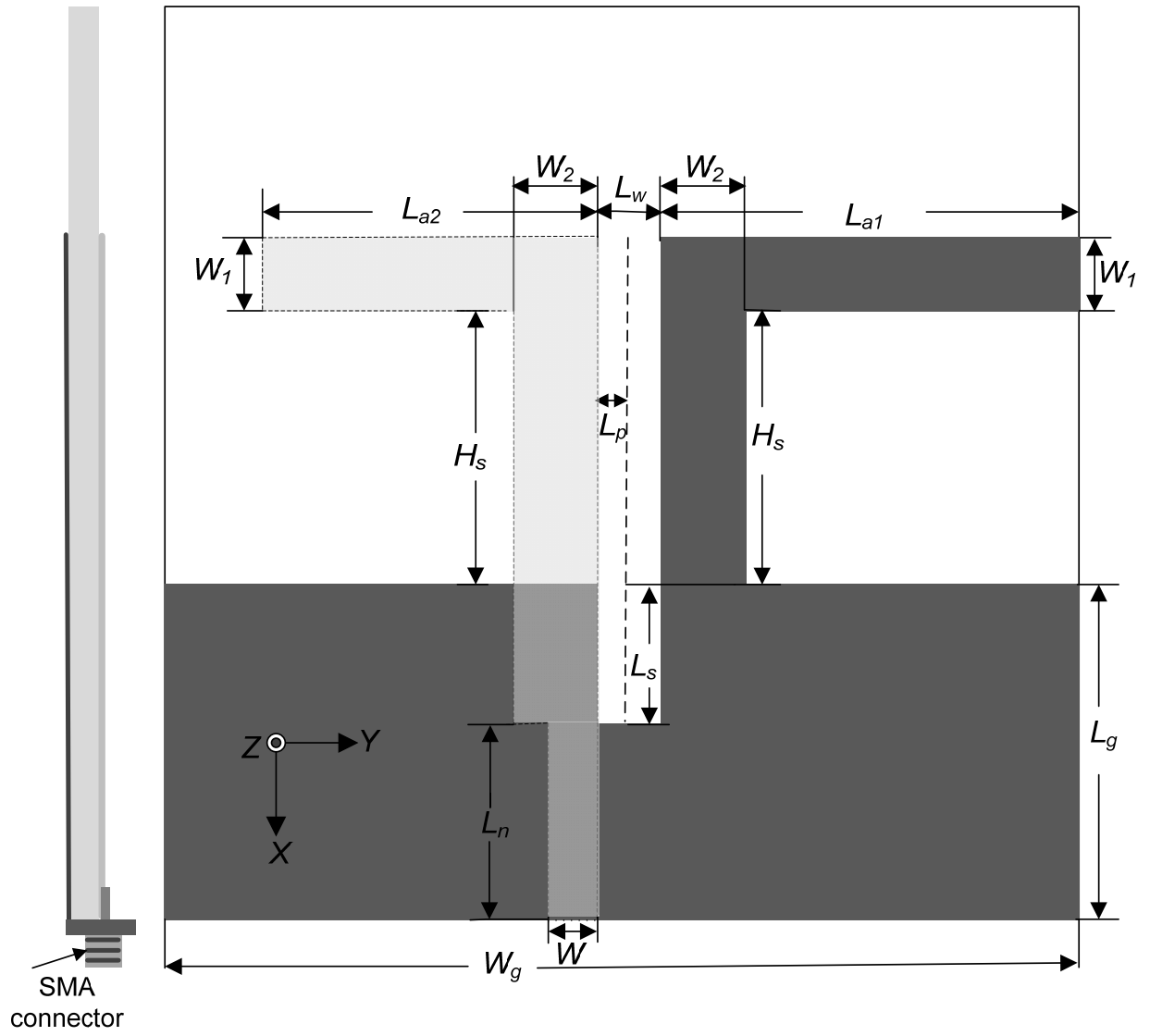
Figure 1.   The geometry and coordinate system of the proposed antenna
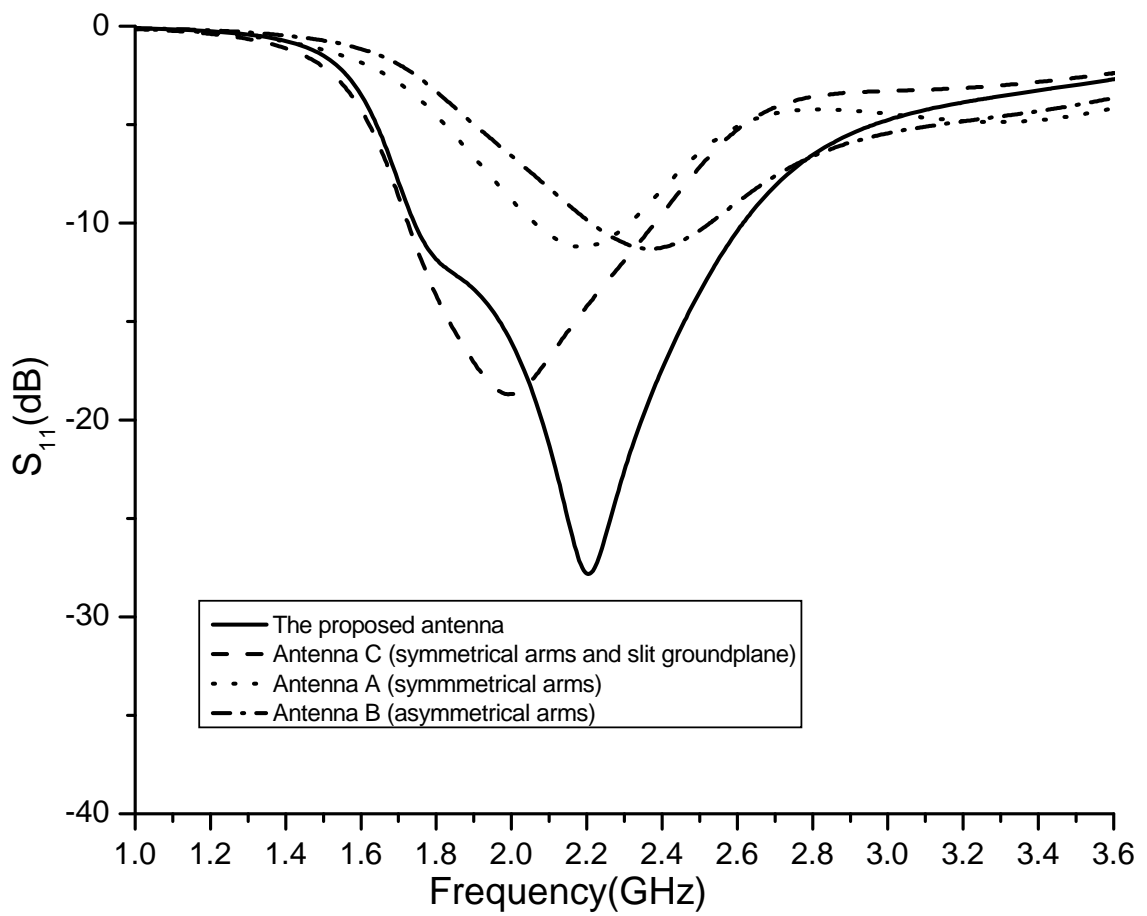
Figure 2. The simulated S_{11} for the printed 4 antenna types.
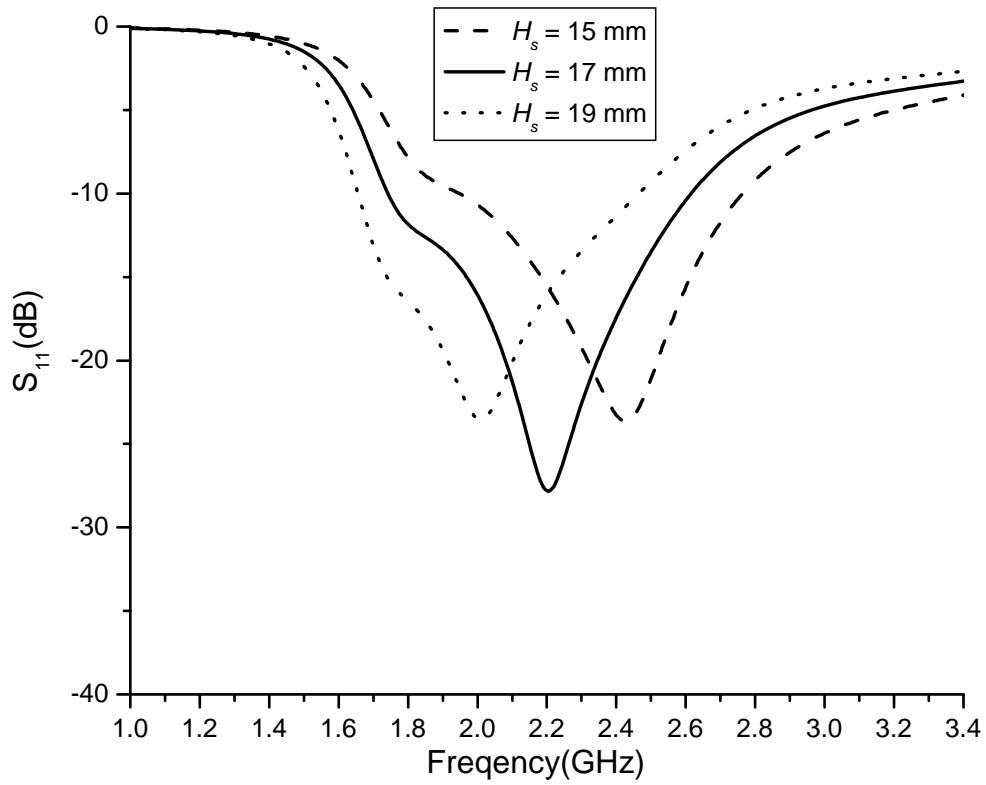
(a)
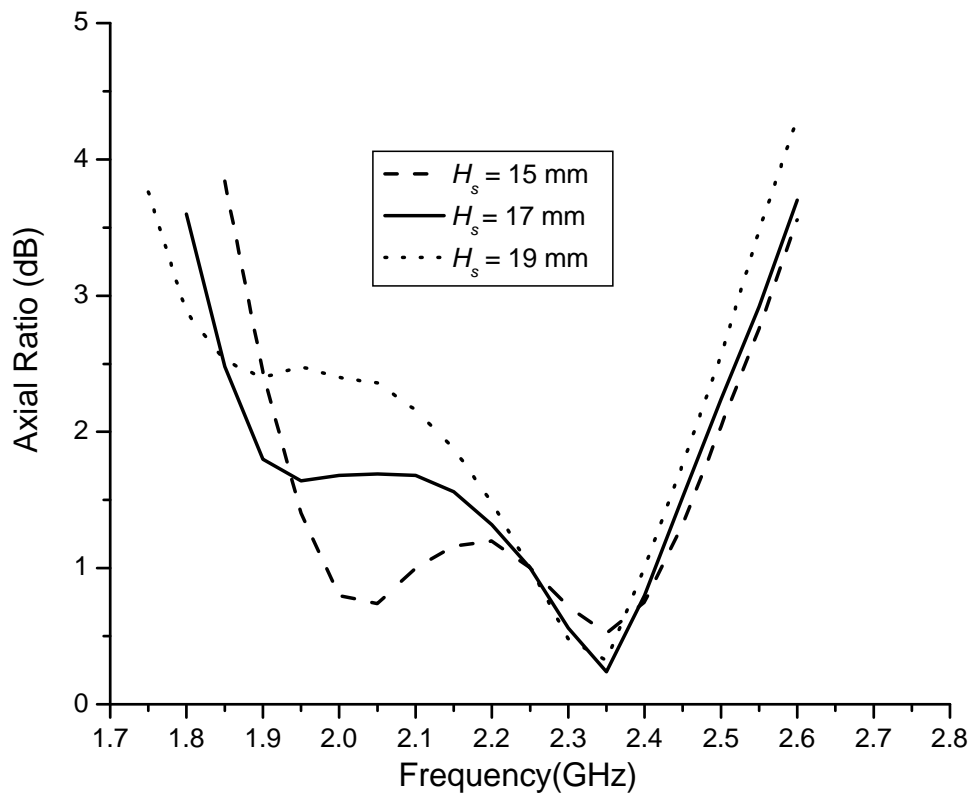
(b)

Figure 3.   The simulated S_{11} (a) and axial ratio (b) for different values of H_s
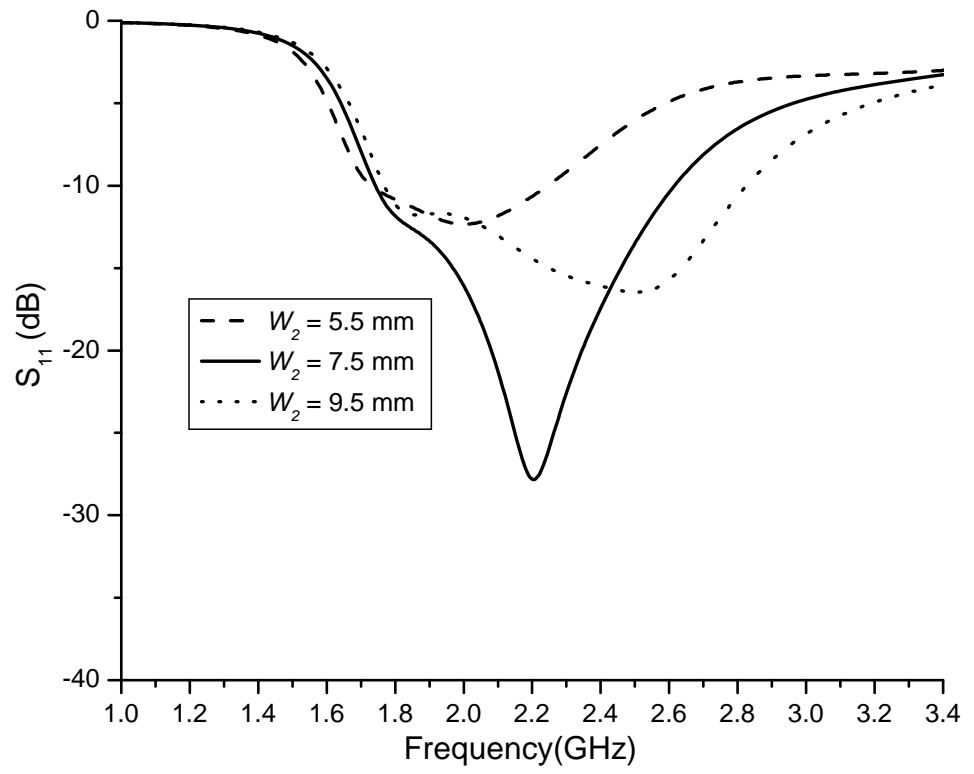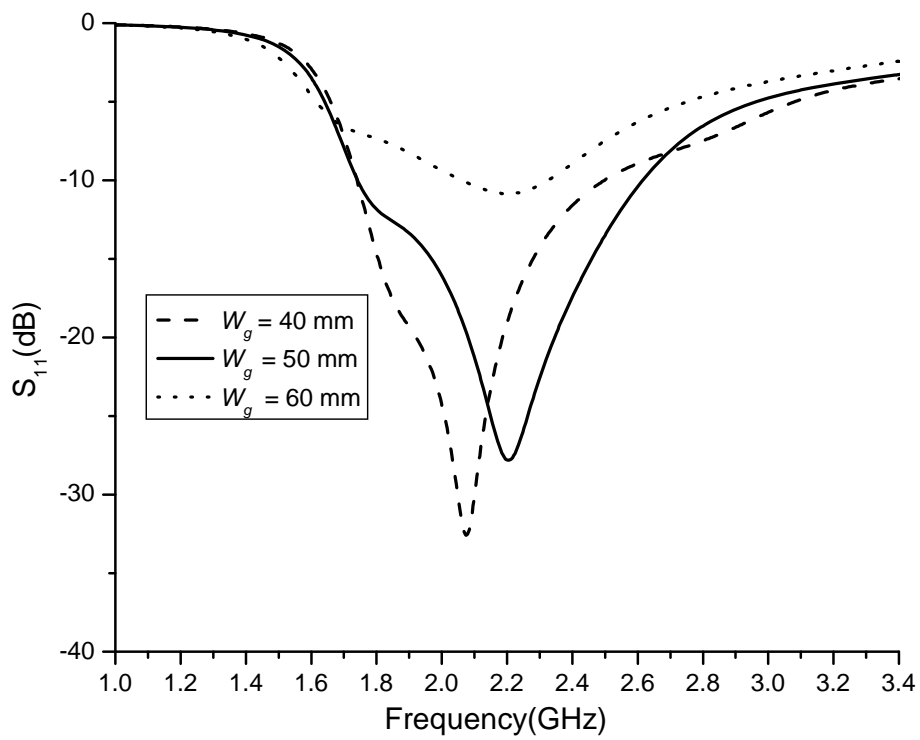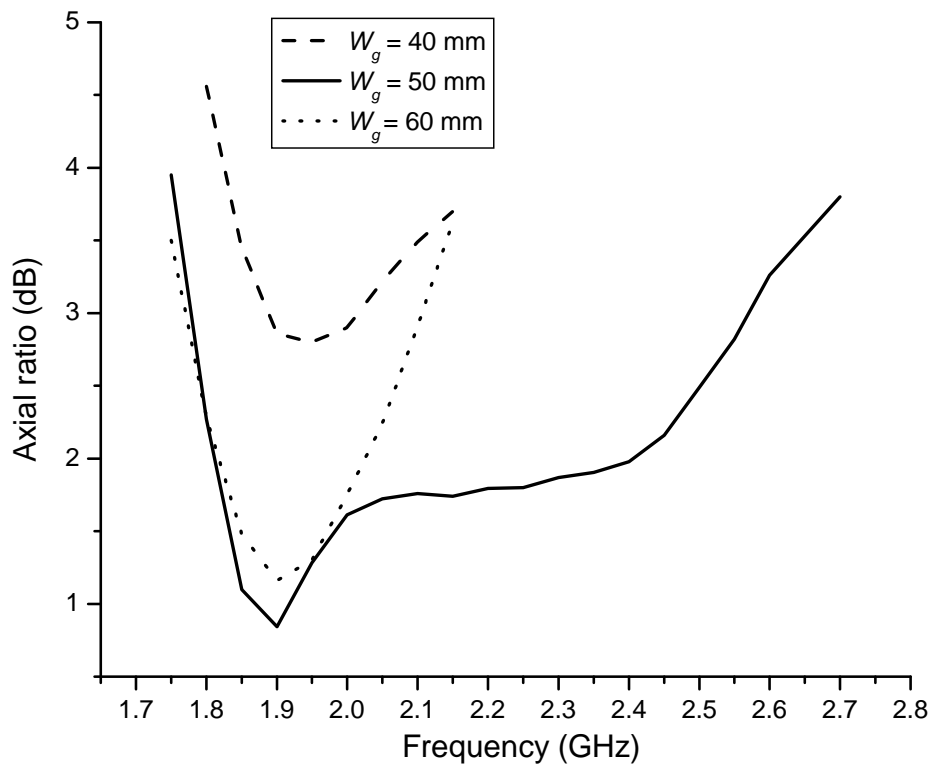
(a)
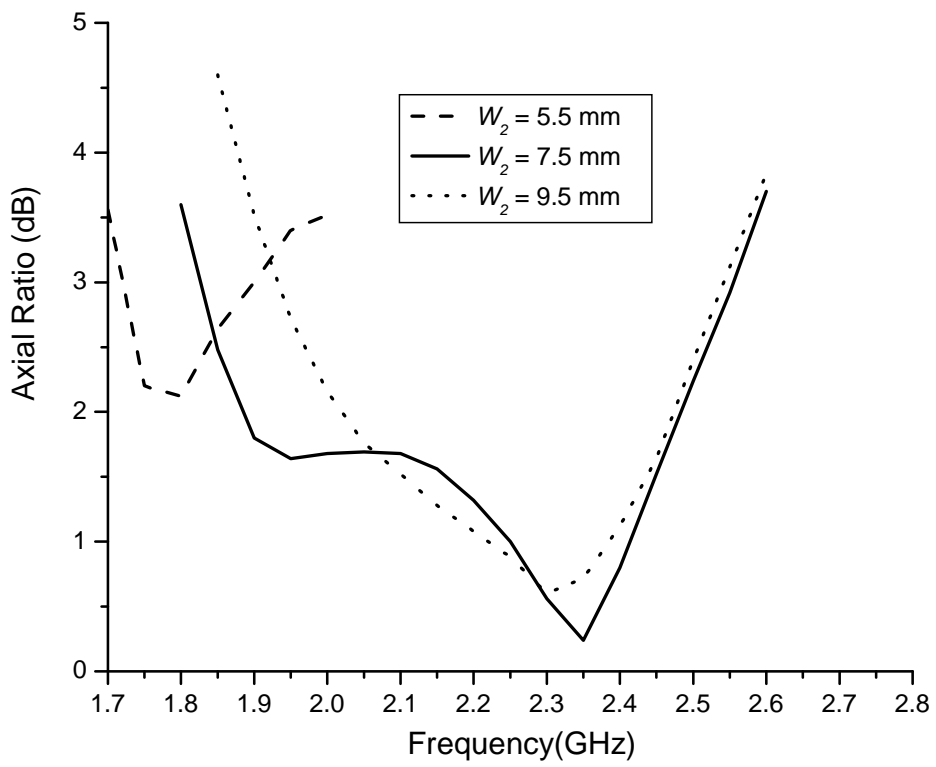
(b)

Figure 4.   The simulated S_{11} (a) and axial ratio (b) for different values of W_2
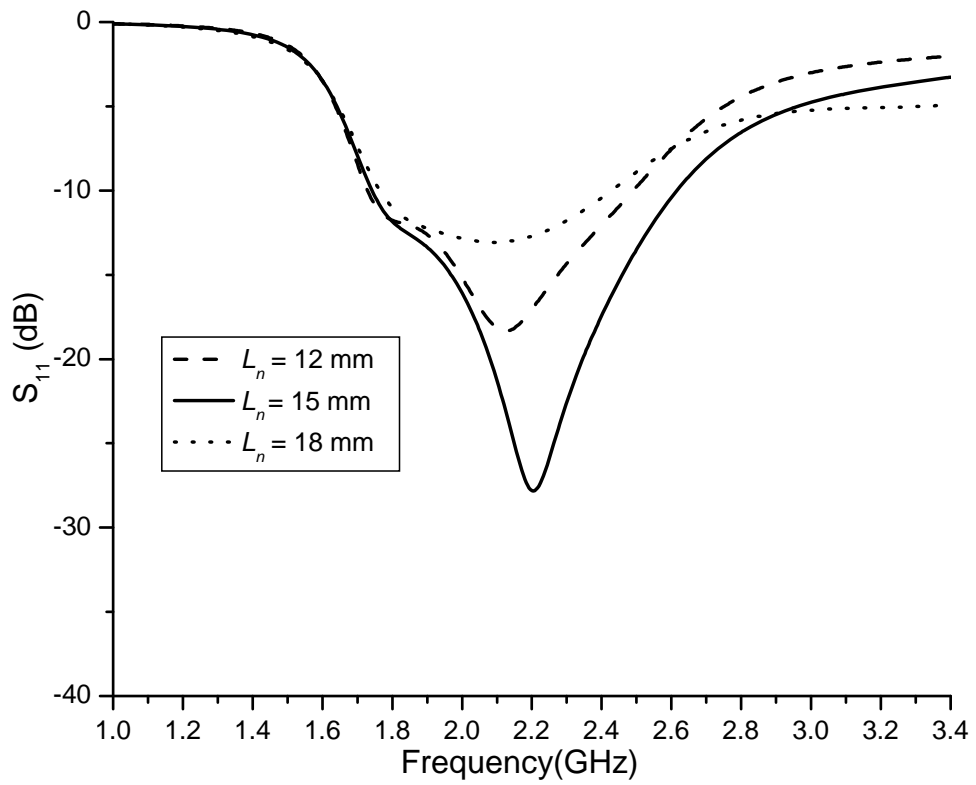
(a)
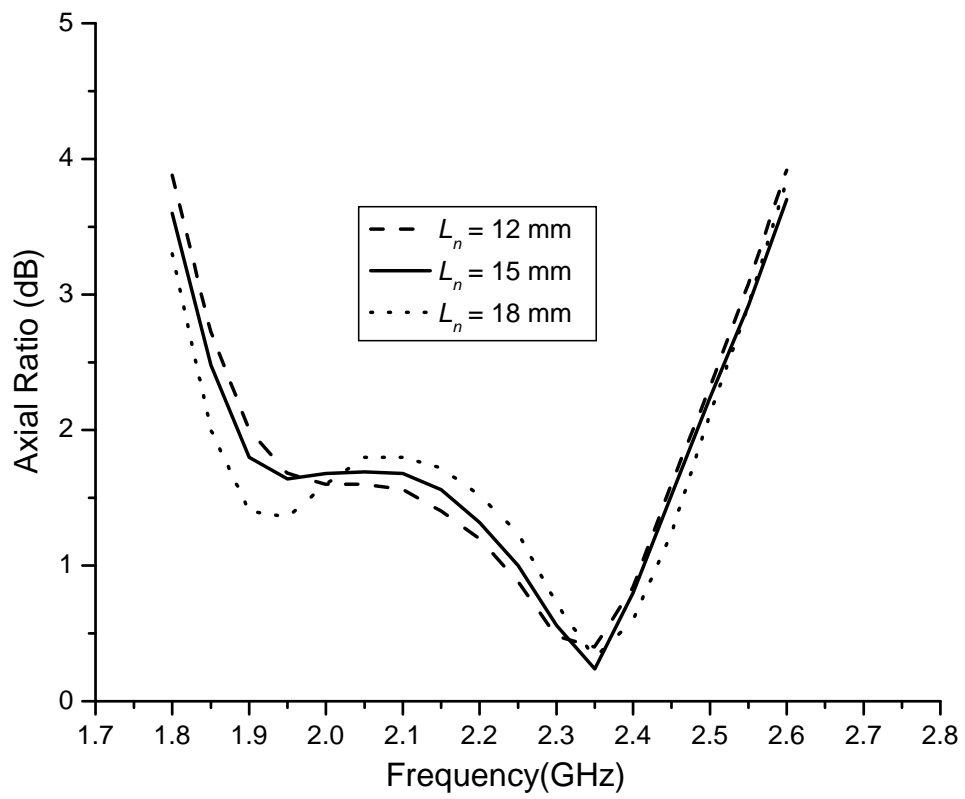
(b)

Figure 5. The simulated S_{11} (a) and axial ratio (b) for different values of L_n
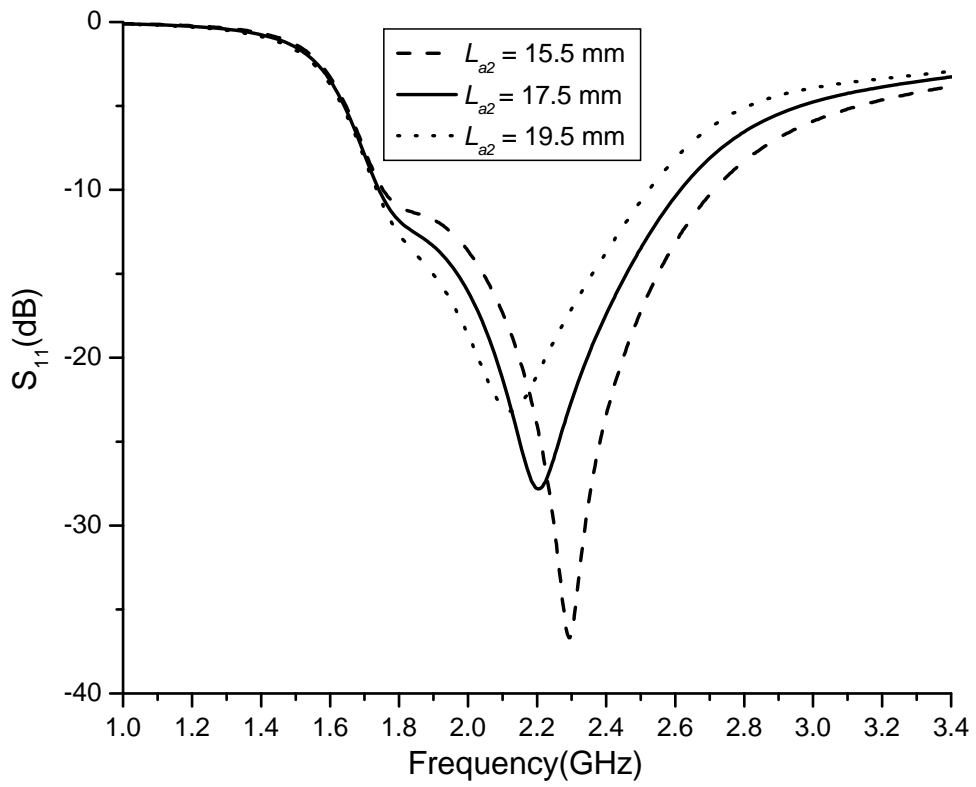
(a)
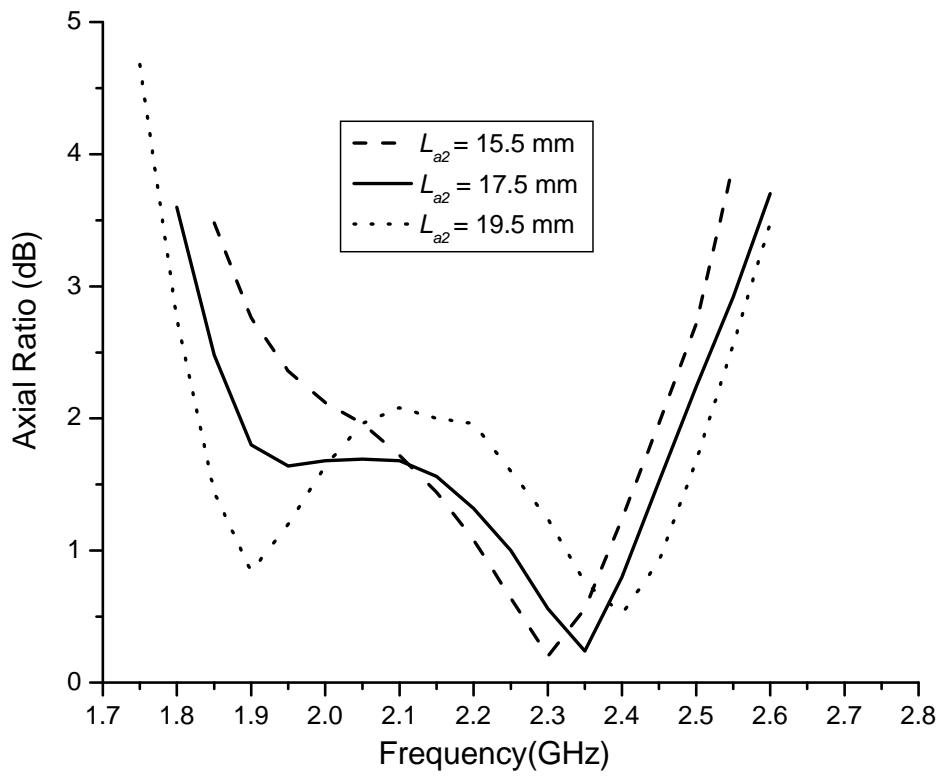
(b)

Figure 6.   The simulated S_{11} (a) and axial ratio (b) for different values of short arm length L_{a2}
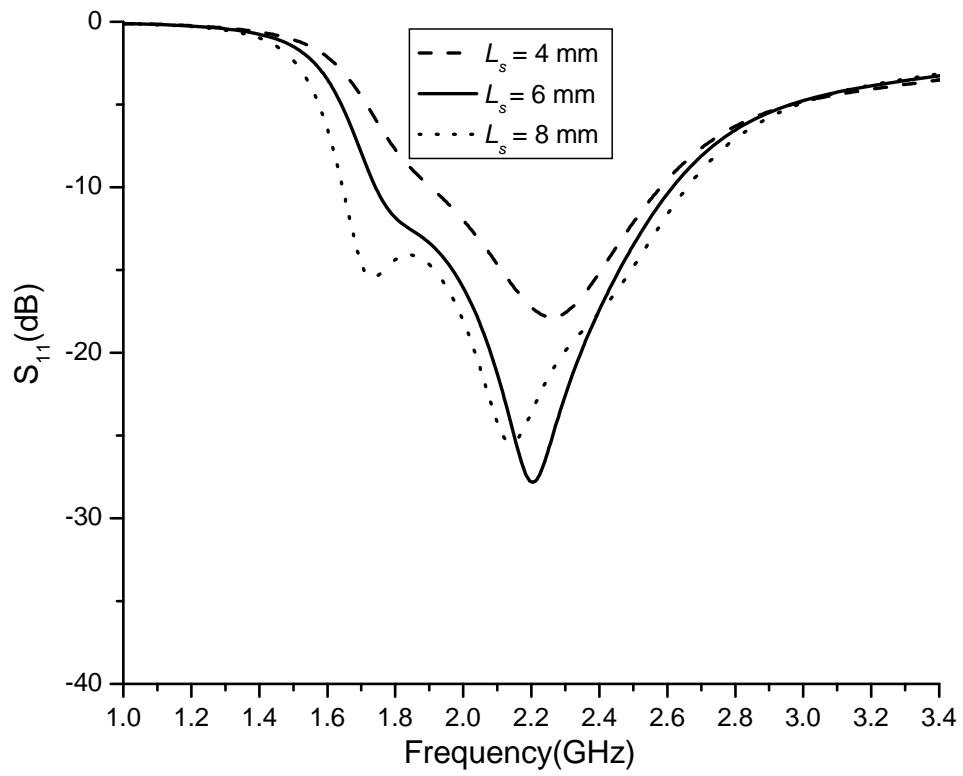
(a)
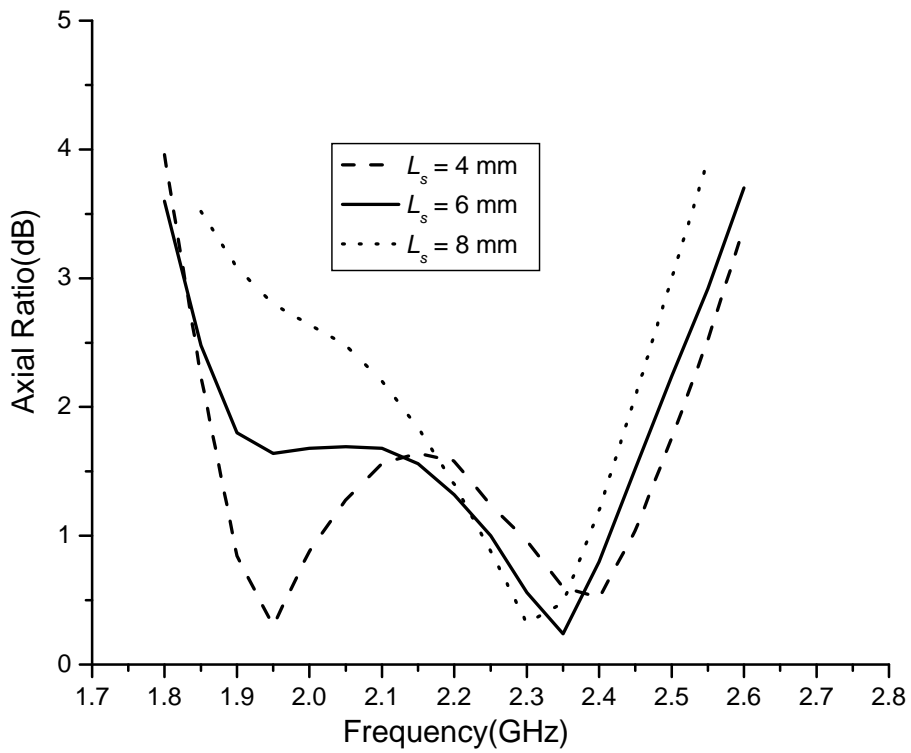
(b)

Figure 7.   The simulated S_{11} (a) and axial ratio (b) for different values of slot length L_s
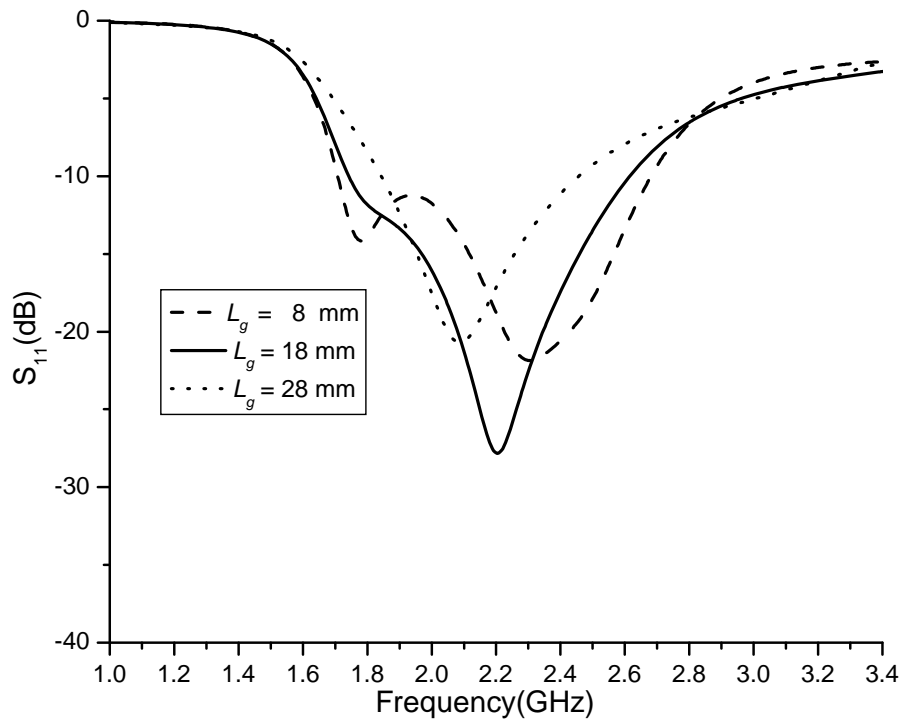
(a)
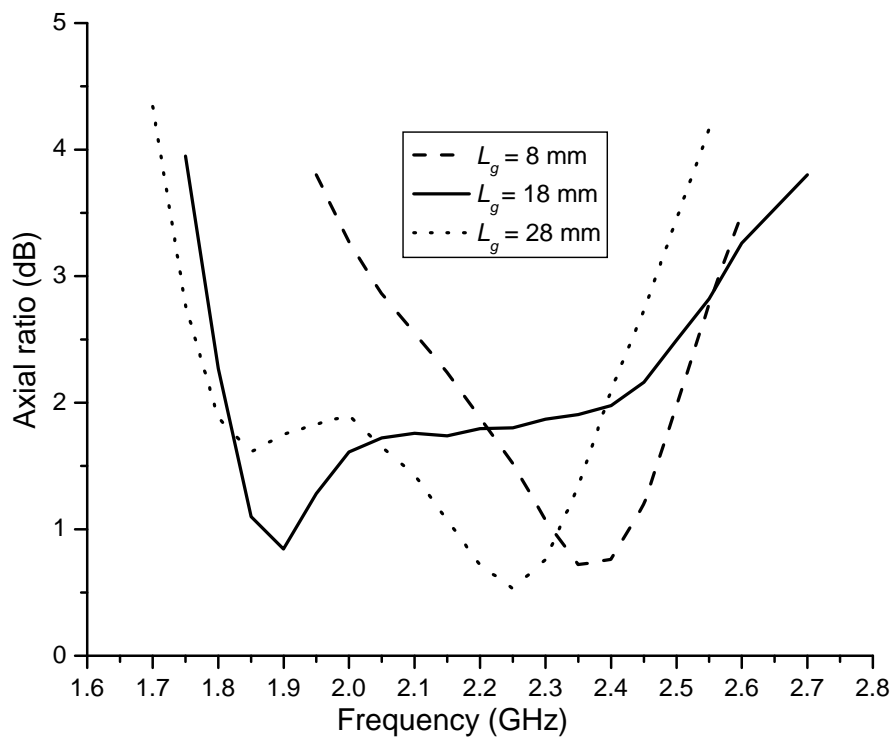
(b)

Figure 8.   The simulated S_{11} (a) and axial ratio (b) for different values of ground plane length L_g

(a)

(b)

Figure 9. The simulated S_{11} (a) and axial ratio (b) for different values of ground plane width W_g
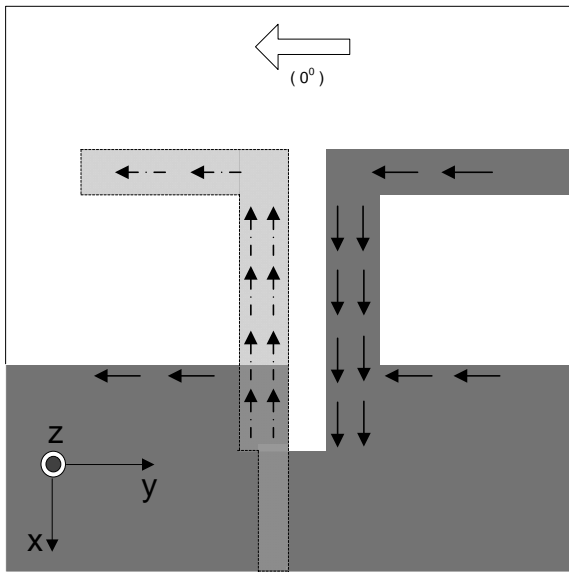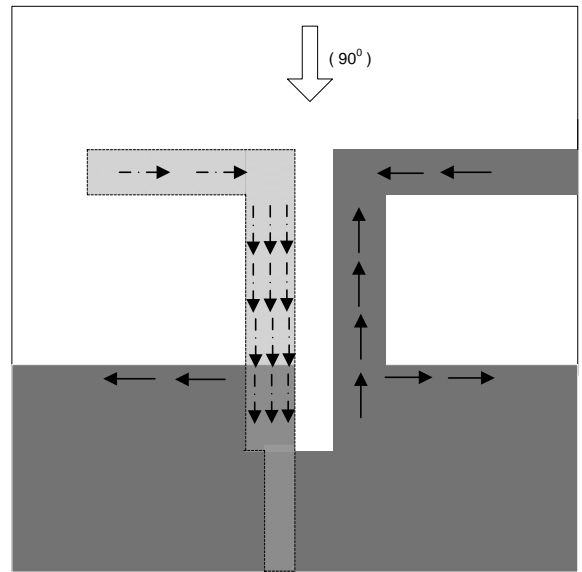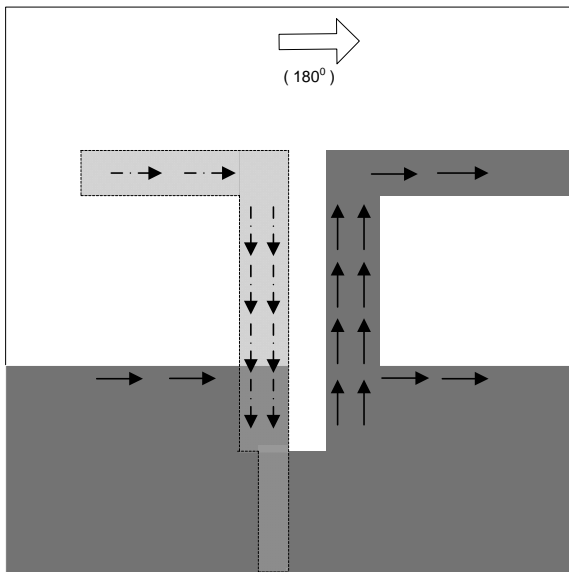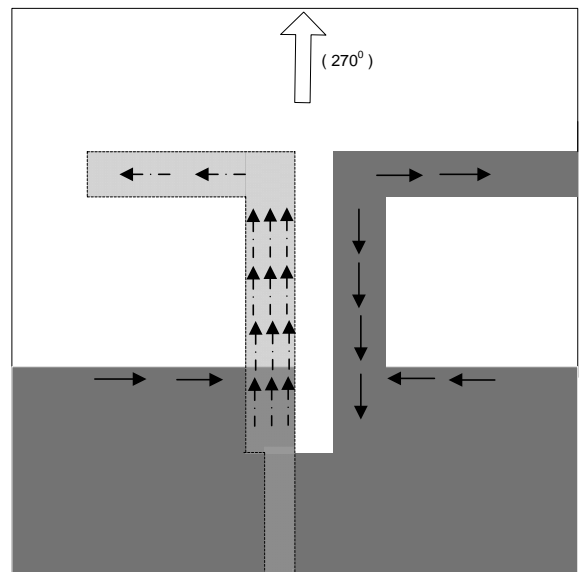
Figure 10.   The simulated current distributions for the proposed antenna (a) 0$^{°}$ phase, (b) 90° phase, (c) 180° phase, (d) 270° phase. The current on the microstrip is that which exists on the exposed side of the line.
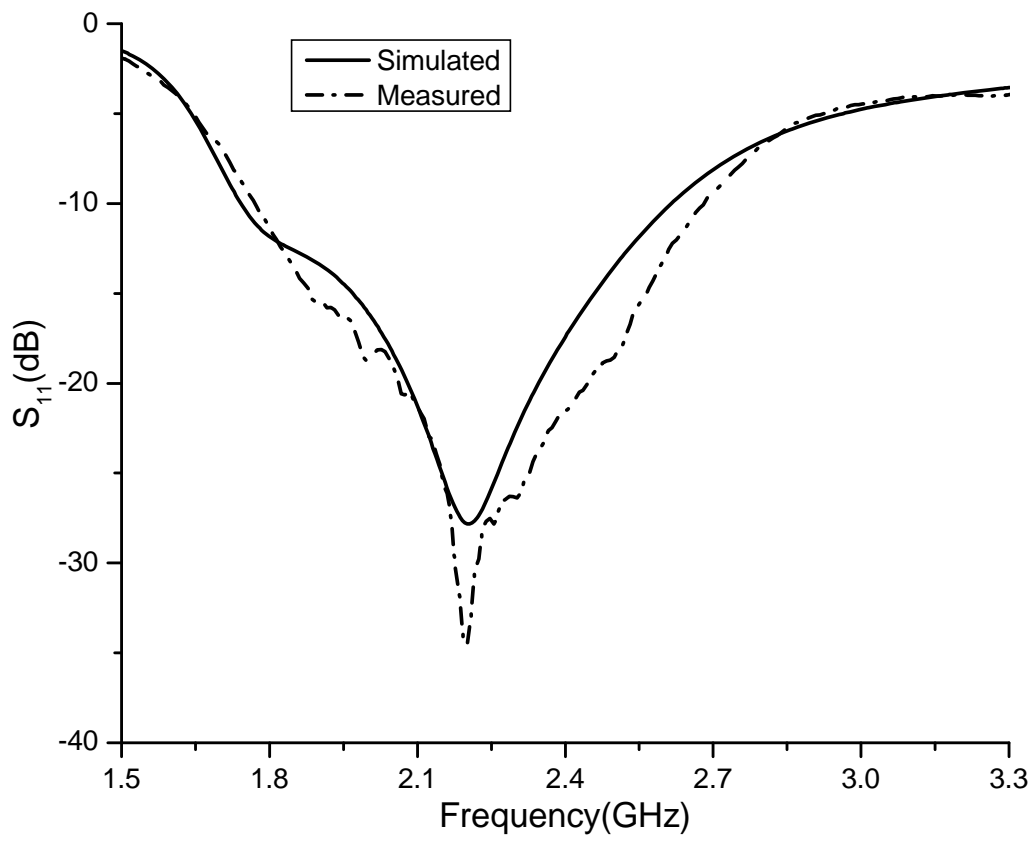
Figure 11.   The simulated and measured S_{11}
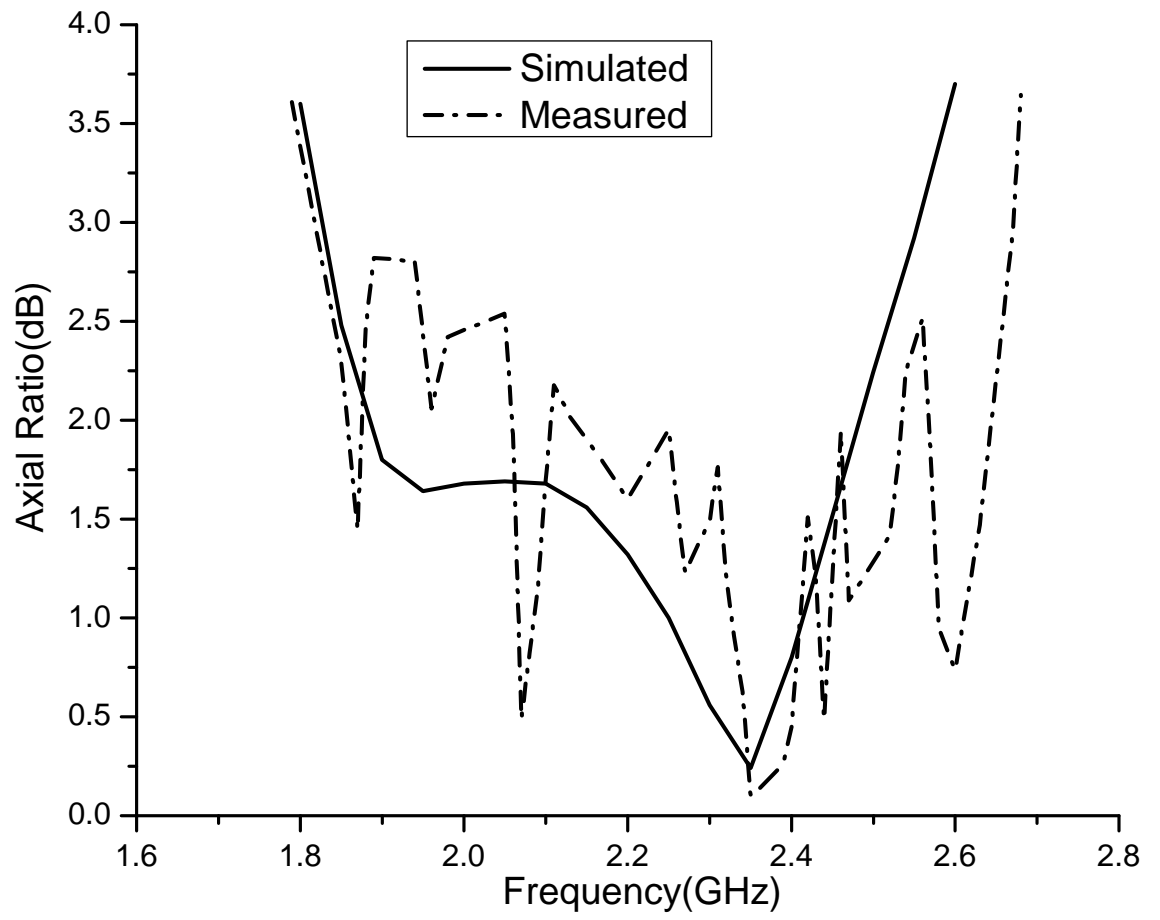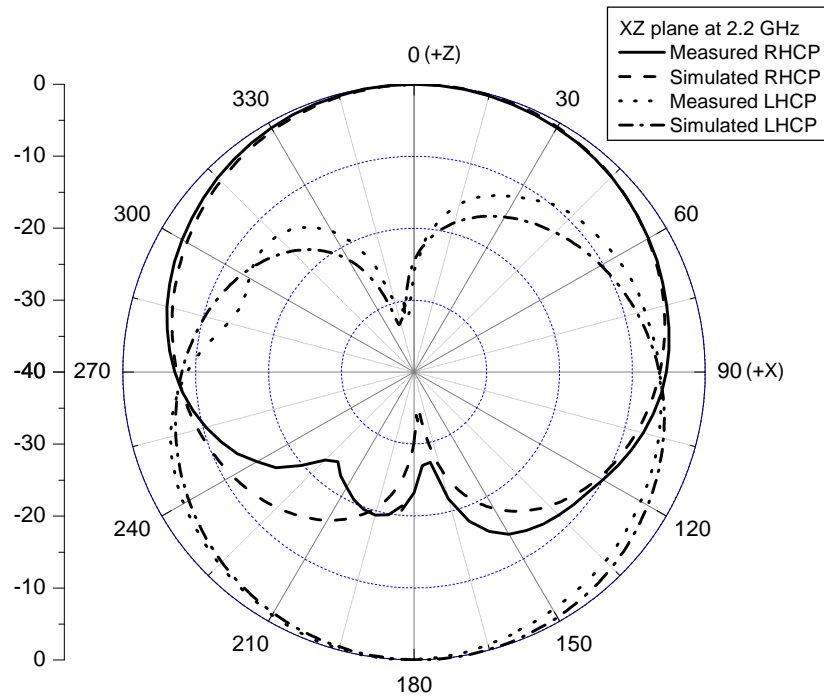
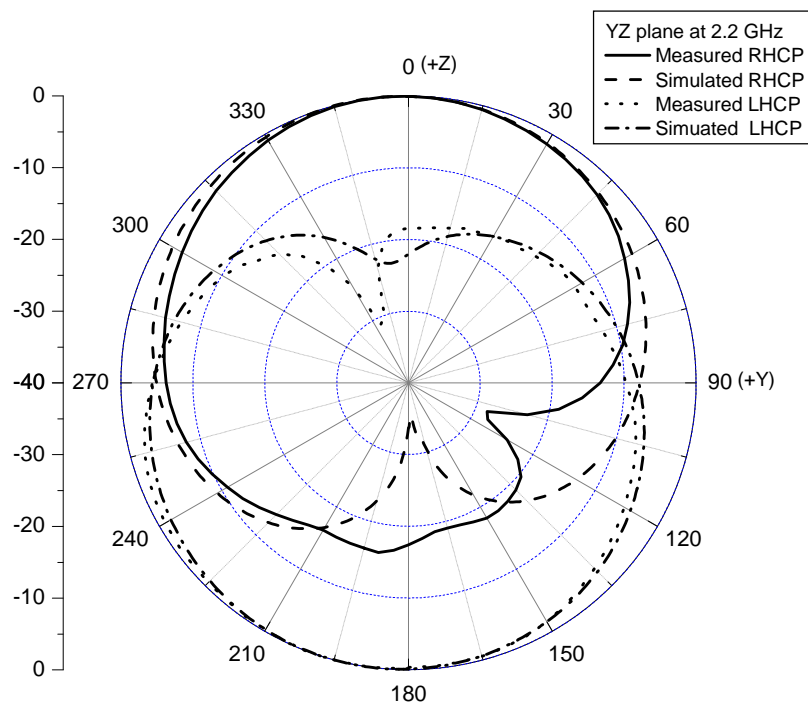Figure 12. The simulated and measured axial-ratio
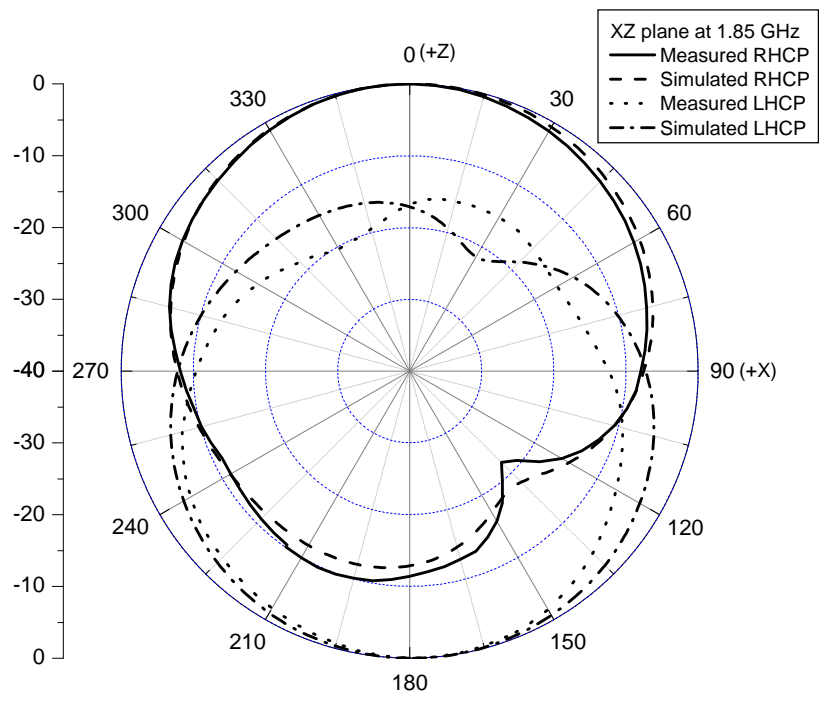
(a)
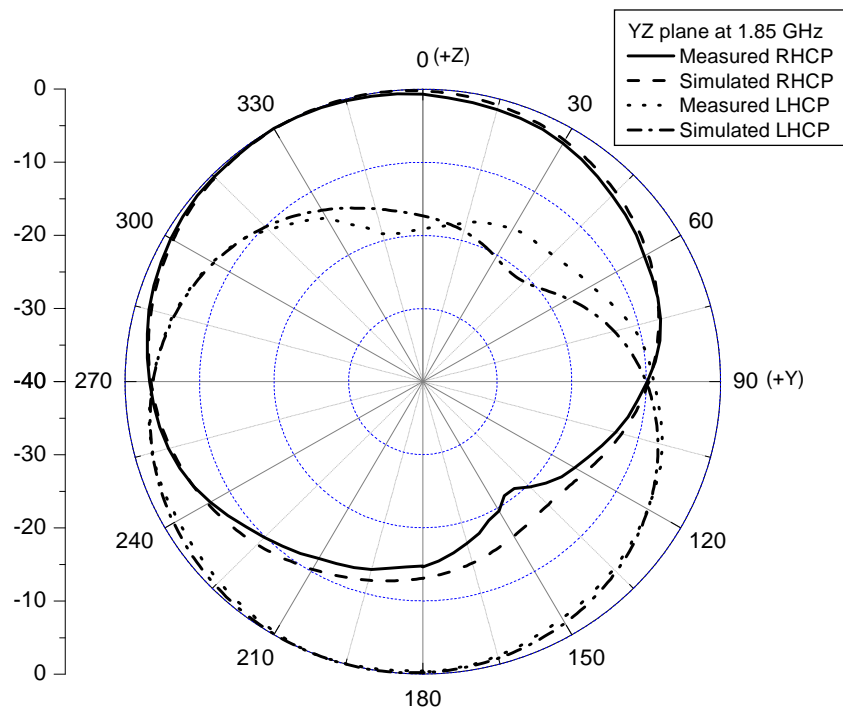
(b)

Figure 13.   The simulated and measured radiation patterns at 1.85 GHz for the (a) XZ plane and (b) YZ plane
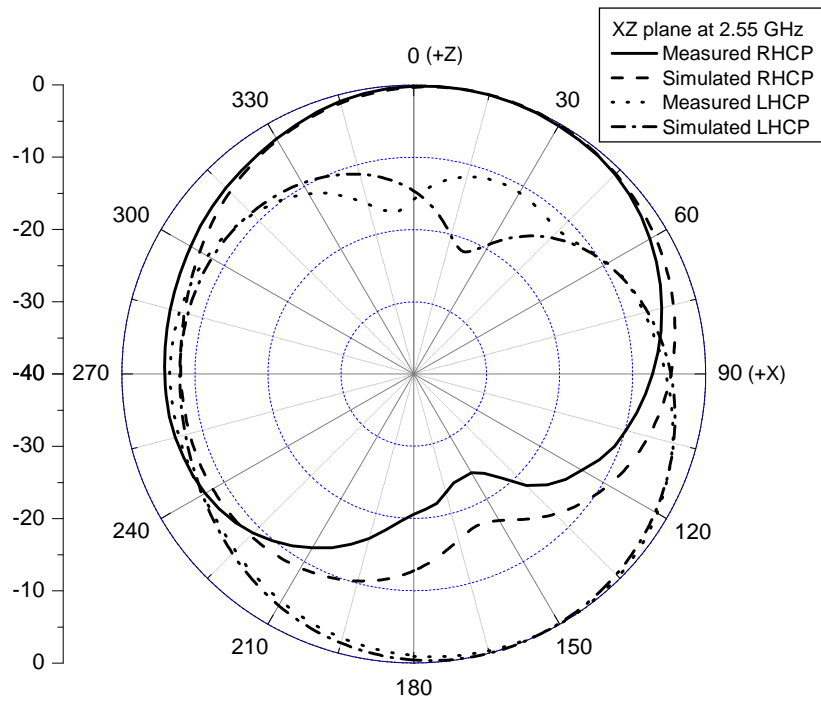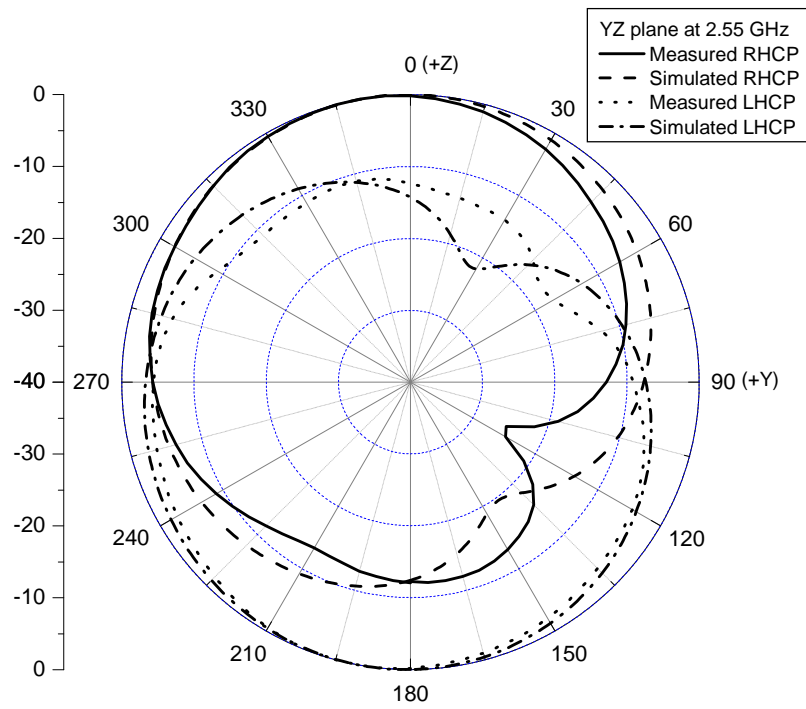
(a)

(b)

Figure 14.   The simulated and measured radiation patterns at 2.2 GHz for the (a) XZ plane and (b) YZ plane

(a)

(b)

Figure 15. The simulated and measured radiation patterns at 2.55 GHz for the (a) XZ plane and (b) YZ plane